Dynamics of solid-liquid interface morphology during high rate crystallization of alloys

N.A. Berjeza, V.I. Mazhukin*, S.P. Velikevitch and I. Smurov**

Physical Technical Institute, Byelorussian Academy of Science, Zhodinkaya St. 4, 220730 Minsk, Byelorussia
* *Institute of Mathematical Modeling, Russian Academy of Science, Miusskaya Square 4, 125047 Moscow, Russia*
** *Ecole Nationale d'Ingénieurs de Saint-Etienne, 58 rue Jean Parot, 42023 Saint-Etienne, France*

Abstract: The paper presents the results of investigation for the dynamics of solid-liquid interface morphology during high rate crystallization in metallic alloys (Armko-iron and titanium alloy) irradiated both with pulsed and CW-laser beams. Mathematical models used in calculating the temperature gradient G, the solidification interface velocity R, and the G/R value at the solid-liquid interface have been considered. Based on the calculated and measured data, a simple procedure for determining the G/R critical values characterizing the transitions from a planar front to a cellular structure and from a cellular to cellular-dendritic structure during solidification has been proposed. The regularities for the rapid solidification process have been studied for the titanium alloy subjected to boriding with a CW-laser.

1. Introduction

The problem of metal and alloy solidification from a liquid phase after laser surface alloying is an integral part of a general problem of solidification. It was calculated that laser irradiation of metals and alloys gives rise to high rates of cooling ($10^4 - 10^6$ K/s) and solidification ($1 - 10^2$cm/s) [1,2]. At such high rates, under appropriate laser treatment, the formation of a planar front, cellular, cellular-dendritic and dendritic structures is observed [1,4]

by analogy with near-equilibrium solidification taking place at velocities of $10^{-4} - 10^{-2}$cm/s [3]. The increase in the cooling rate results in the formation of a highly disperse structure. Characteristic size of a cellular structure, for instance, decreases from $50 - 100\mu$m for equilibrium solidification to $0.2 - 10\mu$m in the case under consideration [5]. Similar behavior was also exhibited for a dendritic structure.

Thus, under high rate solidification and cooling, the same structures (though more disperse), as during near-equilibrium solidification, are being developed. The phase composition, however, differs considerably. The composition of the rapidly cooled metastable allow depends greatly on the heat transfer rate during the solidification process [6,7].

The regularities of solidification front morphology taking place at rates of $10^{-4} - 10^{-2}$cm/s, have been extensively studied by Cahn [3], Chalmers [8] and others since 50 ies. Their key results have been of great importance both for theory and practice. The attempts of practical workers to achieve a planar – and to avoid a cellular solidification front while making compounds, stimulated in the 50 ies – 60 ies the formulation of a theoretical problem of the stability for the solidification planar front [9-15]. This problem is also of great interest for high rates of solidification [16-19].

The liquid-solid interface morphology determines the microstructure of the arising phase, governing the material mechanical properties. The liquid-solid interface morphology is presently a subject of investigation for high cooling rates and large temperature gradients typical for laser treatment [1,2,17,20].

For low rate ($10^{-4} - 10^{-2}$ cm/s) solidification processes in binary alloys, the G/R value (the ratio of the temperature gradient to solidification front velocity) was found to be a governing parameter when going from a planar front to a cellular structure [21]. As for transition from a cellular to dendritic structure, the $(G/R)^{1/2}$ value was found to be the governing parameter for directional solidification in diluted alloys [22].

In [1] it was shown that at high rate ($1 - 10^2$cm/s) solidification, typical of laser-irradiated Ni-alloys, the decrease in G/R may lead to the following changes in the morphological structure of the solid-liquid interface: a planar front $\rightarrow$ cellulars $\rightarrow$ cellular dendrites $\rightarrow$ dendrites.

The procedure for determining the G/R critical values that characterize transitions from a planar front to a cellular structure and further from a

cellular to cellular-dendritic structure is given in [4] for the Ti-alloy: (wt %) Al 4.5, Mo 2.0, V 4.5, Cr 1.0, Fe 0.6. These values are essential for controlling the structure of the alloy surface layer subjected to laser treatment.

Based on physical-mechanical properties of the structure , one can determine what type of structure should be preferred when subjecting the alloy surface to various loads during utilization. An attempt to measure some physical-mechanical properties was made in [4]. It should be noted, however, that experimental investigation of physical-mechanical properties of the structure is not simple, because these properties are affected not only by the structure itself but also by the phase composition.

Based on the G/R parameter, the morphological instability of the solidification interface in the metallic alloys (Armko-iron, titanium alloy) subjected to pulsed- and CW-laser treatments has been studied in the paper.

2. Theoretical models for G/R calculation

Two theoretical models, depending on the treatment procedure, have been used to calculate the temperature gradient G at the solidification interface, the solid-liquid interface velocity R, and the G/R value during solidification after laser surface alloying.

2.1 Pulsed-laser treatment

The approximated model of Greenvald et al. [1], based on a simple physical model, can be applied to the case of pulsed laser treatment.

The laser output energy, absorbed by a thin near-surface layer of the metal, is converted into heat to melt the surface layer. After pulse termination, the previously heated surface layer is cooled due to heat conduction into the bulk. As a result, the liquid-solid interface for some period of time continues to move inside the metal layer. The motion finally stops while the reverse procedure – motion towards the surface – (solidification) – starts.

The key assumption, made to justify the approximated calculation procedure, is to neglect over the latent melting heat. This assumption considerably simplified the problem – by "withdrawing" it from the Stephan-type problems and relating it to the problems of surface heating without phase transition.

The thermophysical properties of the material were assumed to be approximately the same in solid and liquid states. The material was considered to be a homogeneous semi-finite solid. The density of energy distribution over the spot and during the pulse duration was assumed constant. Cooling of the

melted metal was only realized due to thermal conduction. One-dimensional approximation was considered.

The mathematical formulation of the problem has the form [1,23]:

$$\frac{\partial T(z,t)}{\partial t} = a\frac{\partial^2 T(z,t)}{\partial z^2} + \frac{a}{\lambda}q(z,t), \quad q(z,t) = q_{\text{abs}}\delta(z-0)\eta(\tau - t), \quad z > 0, \quad t > 0; \tag{1}$$

$$\lambda\frac{\partial T(z,t)}{\partial z}\bigg|_{z=0} = 0, \quad t > 0; \tag{2}$$

$$T(z,t)|_{t=0} = T_0 = \text{const}, \; z \geq 0; \tag{3}$$

where δ is the Dyrac delta functions and η denotes the Haviside unit function.

The solution of these system of equations upon heating ($t \leq \tau$) and cooling ($t > \tau, \gamma = t - \tau$) has the form [1,23]:

for $t \leq \tau$:

$$T(z,t) = \frac{q_0}{\lambda}\left[\left(\frac{4at}{\pi}\right)^{1/2}\exp\left(-\left(\frac{z}{(4at)^{1/2}}\right)^2\right) - z\,\text{erfc}\left(\frac{z}{(4at)^{1/2}}\right)\right] + T_0,$$

for $t > \tau, \gamma = t - \tau$: (4)

$$T(z,t) = \frac{q_0}{\lambda}\left[\left(\frac{4at}{\pi}\right)^{1/2}\exp\left(-\left(\frac{z}{(4at)^{1/2}}\right)^2\right) - \left(\frac{4a\gamma}{\pi}\right)^{1/2}\exp\left(-\left(\frac{z}{(4a\gamma)^{1/2}}\right)^2\right) - z\left(\text{erfc}\left(\frac{z}{(4at)^{1/2}}\right) - \text{erfc}\left(\frac{z}{(4a\gamma)^{1/2}}\right)\right)\right] + T_0.$$

The values for the temperature gradient $G(z,t)$ and cooling rate $\dot{T}(z,t)$ for the cooling period $t > \tau$ are derived from (4):

$$G(z,t) = \frac{\partial T}{\partial z} = -\frac{q_0}{\lambda}\left[\text{erfc}\left(\frac{z}{(4at)^{1/2}}\right) - \text{erfc}\left(\frac{z}{(4a\gamma)^{1/2}}\right)\right] \tag{5}$$

$$\dot{T}(z,t) = \frac{\partial T}{\partial t} =$$

$$= \frac{q_0}{\lambda}\left[\left(\frac{a}{\pi t}\right)^{1/2}\exp\left(-\left(\frac{z}{(4at)^{1/2}}\right)^2\right) - \left(\frac{a}{\pi\gamma}\right)^{1/2}\exp\left(-\left(\frac{z}{(4a\gamma)^{1/2}}\right)^2\right)\right] \tag{6}$$

$$\dot{T} = G \cdot R. \tag{7}$$

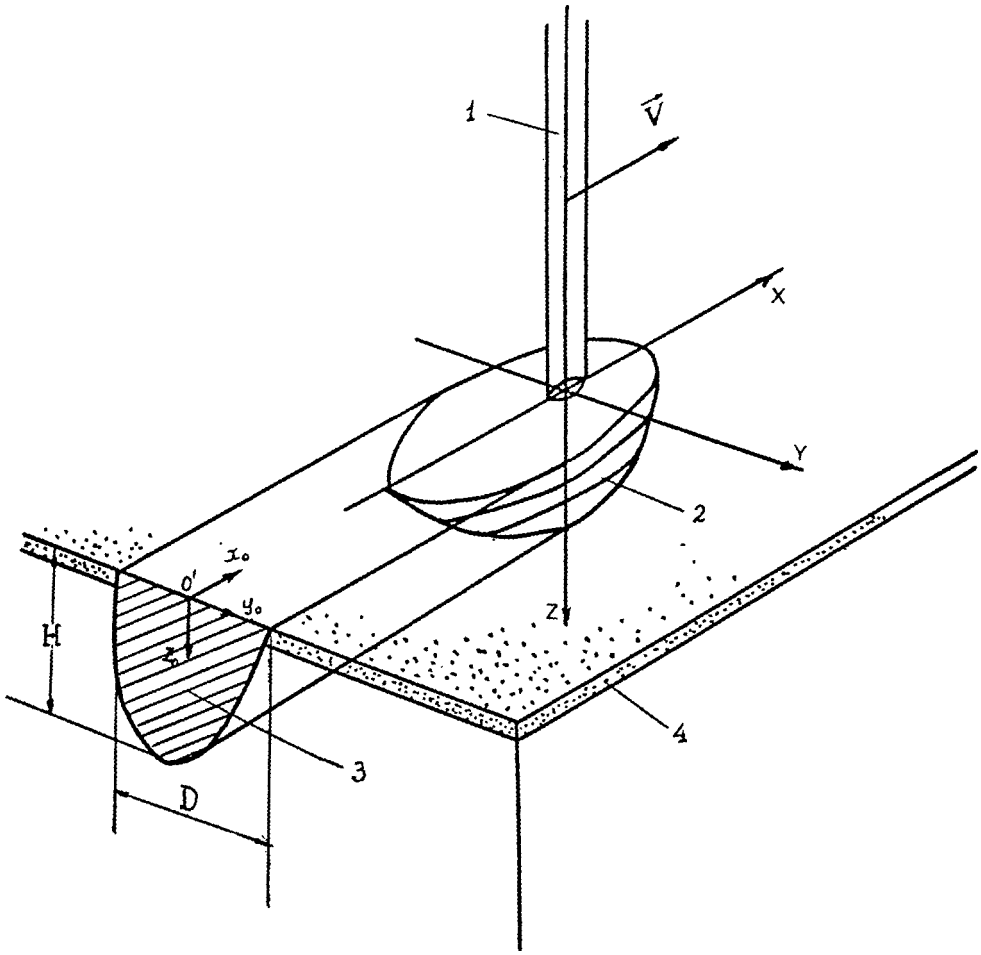

Fig. 1. Scheme of laser boriding process: 1 - laser beam, 2 - isothermal surface $T = T_s$, 3 - cross section of melted bath, 4 - powder coating (boron).

2.2 CW-laser treatment

In case of continuous laser treatment thermal processes can be described by means of the model [25,26]. According to this model temperature fields generated in semifinite domain by Gaussian surface heat source $q = q_{ef}\exp(-(x^2+y^2)/R_{ef})$ moving along the x-axis with velocity V can be described by steady heat transfer equation. In the coordinate system associated with the moving beam the problem is formulated as follows:

$$a\Delta T + V\nabla_x T = 0, \quad x,y \in (-\infty,\infty),\ z \in (0,\infty), \tag{8}$$

$$\lambda\nabla_z T|_{z=0} = -q_{ef}\exp\left(-\left(\frac{x^2+y^2}{R_{ef}^2}\right)\right), \quad q_{ef} = \frac{P_{ef}}{\pi R_{ef}^2}, \tag{9}$$

$$T|_{x=\pm\infty} = T|_{y=\pm\infty} = T|_{z=\infty} = T_0. \tag{10}$$

In dimensionless coordinates and functions

$$f = (T-T_0)\frac{\lambda\pi R_{ef}}{P_{ef}}, \quad \rho = \frac{R_{ef}V}{4a},$$

$$x' = x/R_{ef}, \quad y' = y/R_{ef}, \quad z' = z/R_{ef}$$

the equation system (8) – (10) is looked like the follows:

$$\Delta f + 4\rho\nabla_{x'} f = 0, \quad x',y' \in (-\infty,\infty), z' \in (0,\infty), \tag{11}$$

$$\nabla_{z'} f|_{z'=0} = -exp(-(x'^2+y'^2)), \tag{12}$$

$$f|_{x'=\pm\infty} = f|_{y'=\pm\infty} = f|_{z'=\infty} = 0. \tag{13}$$

Solution of the problem (11) – (13) can be presented in form of the well known integral [25,26]:

$$f(x',y',z',\rho) = \frac{1}{\pi}\int_0^\infty \exp\left[-\frac{(x'+\rho\mu^2)^2+y'^2}{1+\mu^2} - \frac{z'^2}{\mu^2}\right]\frac{d\mu}{1+\mu^2} \tag{14}$$

However direct application of the formula (14) for computations is not convenient because on a number of reasons. The main of them are pointed out below.

1. The function involved to the integral has two peculiarities in the cases $\mu \to 0$ and $\mu \to \infty$. In the case $\mu \to 0$ the rapidly decreasing function $e^{-z'^2/\mu^2}$ is dominant, that places stiff limitations on integration step. When $\mu \to \infty$ the computation process must be restricted by some large value of μ, but error estimation for this operation is very complicate because of large number of parameters (x', y', z', ρ).

2. Procedure of determining of isotherms, temperature maximum and x'-coordinate of the maximum depending on the velocity ρ is cumbersome.

3. There are computational difficulties in determining of temperature fields for planes $y' = \text{const} \neq 0$ and for small values of $\rho, \rho \ll 0$.

To eliminate above mentioned problems it is more convenient to express the solution of the problem (11) – (13) as a product of two functions:

$$f(x', y', z', \rho) = g(r, z', \rho) \cdot exp(\rho^2 - 2\rho x'). \tag{15}$$

Here $g(r, z', \rho)$ describe axissymmetric component of the temperature field and the second term $\exp(\rho^2 - 2\rho x')$ describe additional asymmetric perturbation, which is proportional to asymmetric term $\exp(-2\rho x')$. This new form of presentation for the f function can be derived from formal decomposition into power series in parameter r^2, $r = [(x' - \rho)^2 + y'^2]^{1/2}$. By means of simple but cumbersome transformations the $g(r, z', \rho)$ function can be written in form of integral:

$$g(r, z', \rho) = \int_0^\infty f_1(r, u) \cdot f_2(z', \rho, u)\, du \tag{16}$$

The function involved to the integral is the product of the two function. The $f_1(r, u) = J_0(2ru)$ is the well-known Bessel function which is oscillating and slowly decreasing. The second function $f_2(z', \rho, u)$

$$f_2(z', \rho, u) = \frac{u}{(\rho^2 + u^2)^{1/2}} \exp(-u^2 - 2z'(\rho^2 + u^2)^{1/2})$$

has one maximum on the interval $u \in [0, 1/\sqrt{2}]$ under condition $\rho \neq 0$ and has peculiarity under $u \to \infty$. But the latter peculiarity does not influence

on computations, because variations of the integral $\int_0^{u_\infty} f_2(u)\,du$ are smaller than $\epsilon = 10^{-5}$ for $u_\infty > 4$.

With above consideration taking into account the solution in new form is written as follows:

$$f(x',y',z',\rho) = \exp(\rho^2 - 2\rho x') \cdot \int_0^\infty \frac{u}{(\rho^2+u^2)^{1/2}} \exp(-u^2 - 2z'(\rho^2+u^2)^{1/2}) J_0(2ru)\,du \quad (17)$$

The proposed form of the solution is convenient for numerical computations and eliminate the all mentioned problems.

Absolute value of the interface velocity in the fixed coordinate system (x,y,z) is equal to the normal velocity of the substance "flowing" through the interface in the (x',y',z') coordinate system associated with the moving beam. For steady solidification the interface velocity is expressed as follows (Figure 2):

$$R = V\cos\alpha = V\frac{|\nabla_x T|}{|\nabla T|}\bigg|_{T=T_S} = V\frac{|\partial T'/\partial x|}{|\nabla T|}\bigg|_{T=T_S}. \quad (18)$$

The G/R value at the solidification interface has the form:

$$\frac{G}{R}\bigg|_{T=T_S} = \frac{|\nabla T|^2}{V|\nabla_x|}\bigg|_{T=T_S} = \frac{\left(\frac{\partial T}{\partial x}\right)^2 + \left(\frac{\partial T}{\partial y}\right)^2 + \left(\frac{\partial T}{\partial z}\right)^2}{V\left|\frac{\partial T}{\partial x}\right|}\bigg|_{T=T_S} =$$

$$= \frac{T_s - T_o}{R_{ef}V}\left\{\frac{1}{f}\frac{\left(\frac{\partial f}{\partial x'}\right)^2 + \left(\frac{\partial f}{\partial y'}\right)^2 + \left(\frac{\partial f}{\partial z'}\right)^2}{\left|\frac{\partial f}{\partial x'}\right|}\right\}\bigg|_{f=f_S} \quad (19)$$

The model assumes the overcooling value at the liquid-solid interface to be low. The cooling rate at the solidification front in the fixed coordinate system is expressed via a x'-coordinate derivative of the f function in the moving coordinate system:

$$\dot{T}\,|_{T=T_S} = \frac{\partial T}{\partial t}\bigg|_{T=T_S} = G\cdot R\bigg|_{T=T_S} = -\frac{(T_s - T_0)V}{R_{ef}}\left(\frac{\partial f}{\partial x'}\right)_{f=f_S} \quad (20)$$

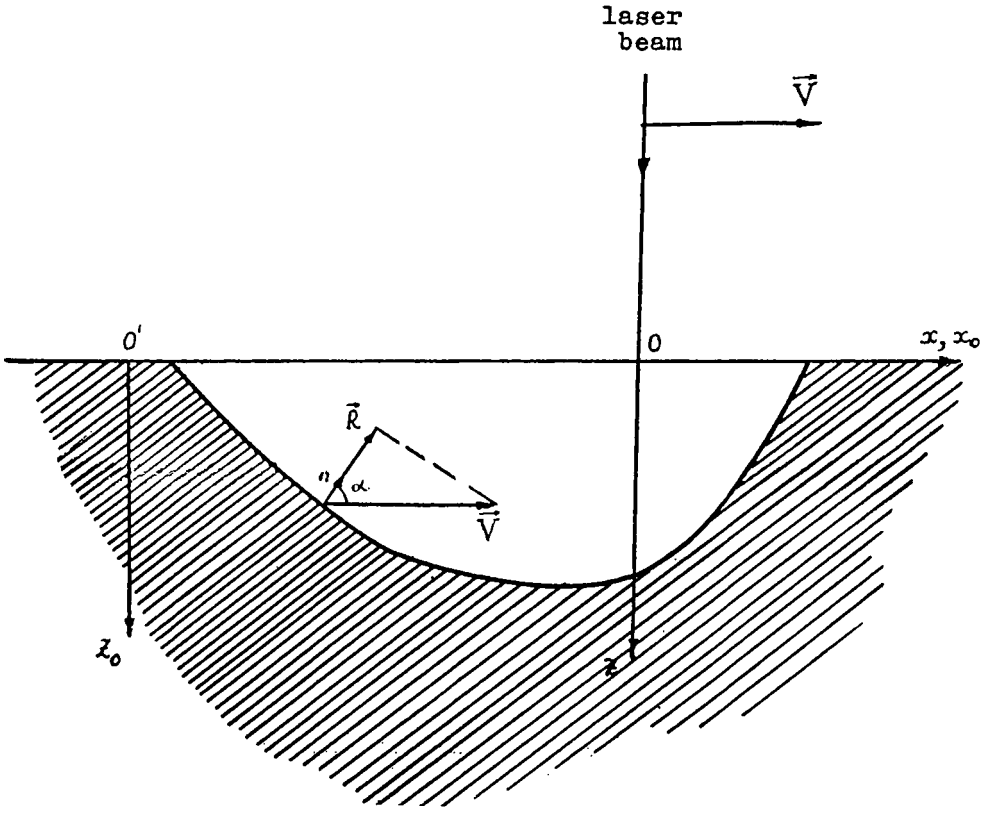

Fig. 2. Longitudinal cross section of specimen.

For the $y' = 0$ plane the G/R expression simplifies and in coordinate system $(r = x' - \rho, z')$ has the form:

$$\left.\frac{G}{R}\right|_{y'=0,\, f=f_S} = \frac{T_s - T_o}{R_{ef} V}\left\{\frac{1}{f_0}\frac{\left(\frac{\partial f_0}{\partial r}\right)^2 + \left(\frac{\partial f_0}{\partial z'}\right)^2}{\left|\frac{\partial f_0}{\partial r}\right|}\right\}\Bigg|_{f_0=f_S} \tag{21}$$

Here

$$f_0(r,z',\rho) = f(x',y',z',\rho)|_{y'=0} = \exp(-\rho^2+2\rho r)\int_0^\infty \frac{u}{(\rho^2+u^2)^{1/2}} F_{exp}\cdot J_0(2ru)\,du,$$

$$\frac{\partial f_0}{\partial z'} = -2\exp(-\rho^2+2\rho r)\int_0^\infty \frac{u}{(\rho^2+u^2)^{1/2}} F_{exp}\cdot J_0(2ru)(\rho^2+u^2)^{1/2}\,du,$$

$$\frac{\partial f_0}{\partial r} = \frac{2}{r}\exp(-\rho^2+2\rho r)\int_0^\infty \frac{u}{(\rho^2+u^2)^{1/2}} F_{exp}\cdot J_0(2ru)\ \times \tag{22}$$

$$\times\left\{\rho r - 1 + u^2 + z'\frac{u^2}{(\rho^2+u^2)^{1/2}} + \frac{u^2}{(\rho^2+u^2)^{1/2}}\right\} du$$

$$F_{exp} = \exp(-u^2 - 2z'(\rho^2+u^2)^{1/2}).$$

To simplify the procedure of finding the points lying on the solidification isotherm $z' = z'(r)$, it is described by following ordinary differential equation:

$$\frac{dz'}{dr} = -\frac{\left(\frac{\partial f_0}{\partial r}\right)\Big|_{f_0=f_S}}{\left(\frac{\partial f_0}{\partial z'}\right)\Big|_{f_0=f_S}}; \quad z'(r=r_0)=0. \tag{23}$$

The equation is solved using the Runge-Kutta procedure where r_0 is determined from the equation $f_0(r_0,0,\rho) = f_s$ by means of Newton iterations.

3. Calculated results

3.1. Pulse laser treatment.

Consider pulsed laser irradiation of Armko-iron ($\lambda = 0.46$ W/cm K, $a = 0.092$ cm^2/s). Three pars of values for q_{abs} and τ where chosen in such a way the initial melt depth H to be the same at the moment of pulse termination, H=24 μm:

1. $q_{abs} = 5\cdot10^5 \mathrm{W/cm^2}$, $\tau = 8.9\cdot10^{-5}$s;
2. $q_{abs} = 5\cdot10^4 \mathrm{W/cm^2}$, $\tau = 2.5\cdot10^{-3}$s;
3. $q_{abs} = 5\cdot10^3 \mathrm{W/cm^2}$, $\tau = 1.2\cdot10^{-1}$s.

For all cases the values of temperature gradient G, cooling rate $\dot{T}$, solidification velocity R and ratio G/R on the interface were numerically determined using (5)-(7), Figure 3.

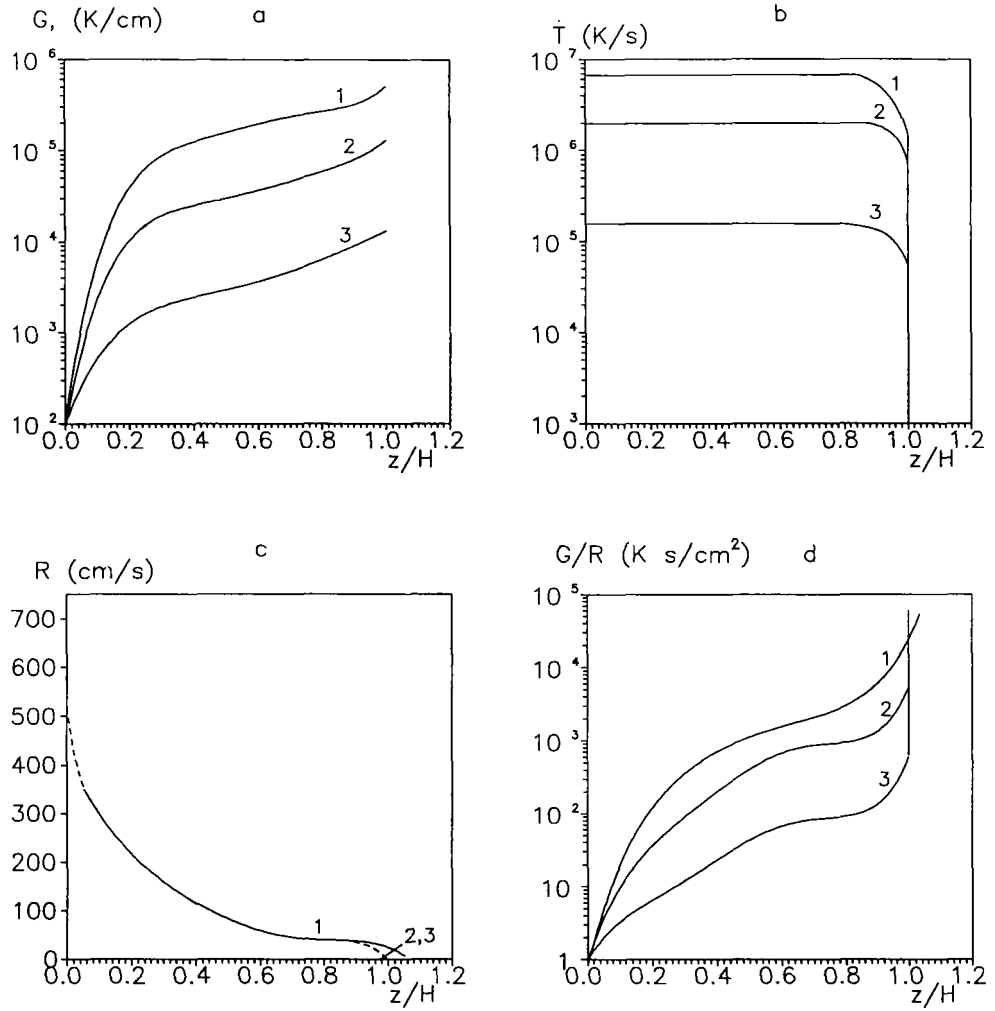

Fig. 3. The dependence of the temperature gradient G (a), the cooling rate $\dot{T}$ (b), the solidification interface velocity R (c) and the ratio G/R (d) at the solidification interface in Armco-iron versus dimensionless melt depth z/H for following values of absorbed power density: $1-q_{abs}=5\cdot10^5\mathrm{W/cm^2}; 2-q_{abs}=5\cdot10^4\mathrm{W/cm^2}; 3-q_{abs}=5\cdot10^3\mathrm{W/cm^2}(H=24\mu\mathrm{m})$.

The plots should be read from the left to the right since $z/H = 1$ corresponds to the start of solidification while $z/H = 0$ corresponds to its end. The $G, \dot{T}, G/R$ values are, in fact, negative for the solidification process but for the convenience are shown as positive. Figure 3a shows the temperature gradient at the solidification interface to be maximum at the initial moment of solidification and to approach zero at the end. Nearly a linear dependence on z/H is observed for z/H values from 0.8 to 0.3. As indicated by Figure 3a,b,d, for the constant initial depth of the melted layer H, the temperature gradient G, cooling rate $\dot{T}$ and G/R value are directly proportional to the absorbed power density q_{abs}. At the onset of solidification the cooling rate $\dot{T}$ "start" from zero, then increases abruptly, and finally at z/H=0.8 achieves a constant value, Figure 3b. The solidification velocity R is independent on q_{abs} for enough large values of H (Figure 3c). The only slight difference in the solidification velocity is observed at the earliest steps of solidification, at $z/H = 1$. In Armko-iron, with the solidification interface moving towards the surface, R increases from 0 (at $z/H = 1$) to 40 cm/s ($z/H = 0.9$) achieving hundreds of centimeters per second at $z/H \to 0$. This model is very approximate and, as shown in [20], with the latent melting heat taken into account, the R value by reaching the "plato" (40 cm/s for Armko-iron) remains constant up to the end of the solidification process. Let us focus at the G/R value at the solidification interface, as this value is important parameter for the formated morphological structure. Figure 3d shows that the G/R value starts to change from ∞ at the onset of solidification ($R = 0, G$ is at maximum) exhibiting a nearly linear dependence on the dimensionless depth at z/H in the range from 0.8 to 0.3. Further the G/R curve changes its curvature and, finally, at the end of solidification the G/R value approaches 0 (since $G \to 0$ and R is at maximum).

3.2. CW – laser treatment.

Let us now turn to the case of continuous laser treatment. Computations for the Ti alloy (wt %) Al 4.5, Mo 2.0, V 4.5, Cr 1.0, Fe 0.6 ($\lambda = 0.21$ W·cm/K, $a = 0.07$ cm$^2/s$, $T_{\text{melt}} = 1933K$) were performed for three groups of laser beam parameters, (Table 1). Numerical results were determined using (11,12), (Figure 4).

Table 1. The values of the P_{ef} and R_{ef} parameters for Gaussian surface heat source for different velocities of laser beam.

Experimental data				Calculated data	
Laser beam velocity V, m/min	Laser beam power P, kW	Depth of melted zone H, mm	Width of melted zone D, mm	Effective power of source P_{ef}, kW	Effective radius of source R_{ef}, mm
0.5	1	0.550	1.950	0.264	0.767
1.0	1	0.375	1.500	0.235	0.668
2.0	1	0.280	1.400	0.292	0.755

Figure 4 shows G/R and $\dot{T}$ at the solidification interface on the plane $y = 0$ as a function of the dimensionless depth of melted layer z/H, computed for the following values of laser beam velocity: $V = 0.5$ m/min , 1 m/min , 2 m/min.

Common behavior of the G/R value at the solidification interface is appeared to be approximately the same for continuous (Figure 4b) and pulse (Figure 3d) laser treatment. At the onset of solidification the G/R value is maximum. At z/H amounting from 1.0 to 0.9 G/R decreases abruptly and then decreases smoothly up to a certain finite V-dependent value at z/H ranging from 0.9 to 0. As evident from Figure 4a , G/R is dependent on the laser beam velocity V: the values of G/R are smaller for the greater values of V.

The dependence of the cooling rate $\dot{T}$ on z/H at the solidification interface for continuous laser treatment (Figure 4b) coincides with that for pulsed laser treatment (Figure 3b). The cooling rate $\dot{T}$ "start" from zero at the onset of solidification , then increases abruptly at z/H ranging from 1.0 to 0.9. At z/H amounting from 0.9 to 0, the $\dot{T}$ changes slowly.

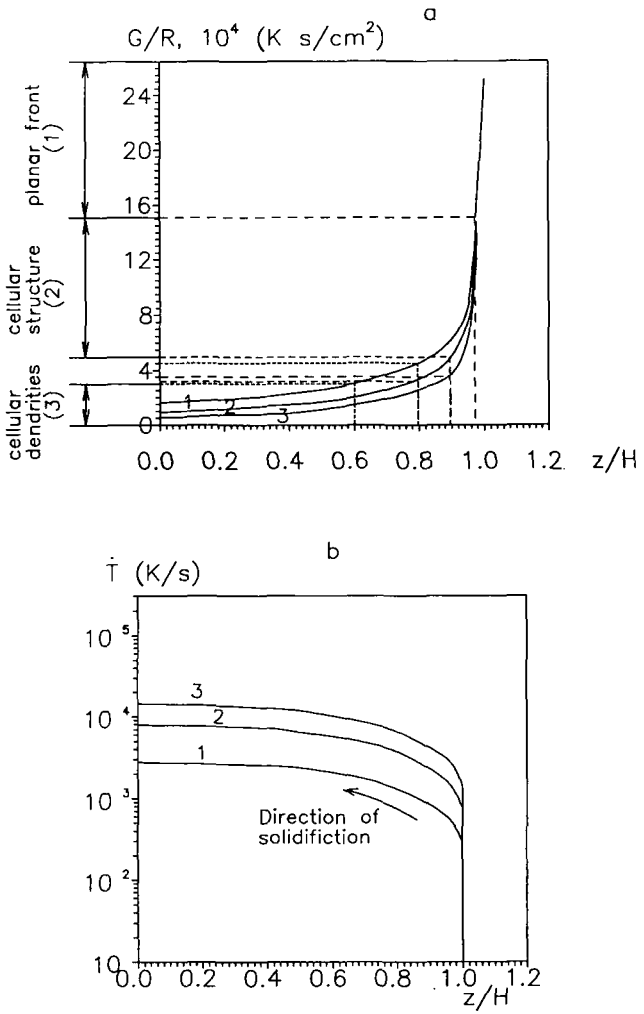

Fig. 4. The dependence of G/R (a) and $\dot{T}$ (b) versus dimensionless melt depth z/H at the interface in the plane $y = 0$: 1 - $V = 0.5$ m/min , 2 - $V = 1.0$ m/min , 3 - V=2.0 m/min.

4. Computation of (G/R) critical values

The measured data of solidification morphological structure were used to calculate critical values $(G/R)_{cr}$ that characterize the transitions in the Ti alloy: a planar front → a cellular structure → cellular-dendritic structure [4] (Figure 5). In the experiment, the specimens of the annealed titanium alloy (wt %) Al 4.5, Mo 2.0, V 4.5, Cr 1.0, Fe 0.6, previously coated with the amorphous boron powder, were irradiated with a continuous CO_2-laser in argon environment. For the experiment 1 kW laser output power, 1 mm focusing spot radius and 0.5 - 2.0 m/min beam velocity were used. A "Neophot -21" optic microscope and a "JSM−35c" rastr electronic microscope were used to study the laser-treated zones [4]. Each laser-affected specimen was furthers cut normal to the direction of the laser beam motion. Then the depths of the transitions from one type of structure to another were measured using obtained cross-section of the melt $(y_0\,0\,z_0)$ (Figure 1).

The transition from a planar front to a cellular structure was distinctly observed through the optic microscope for the laser beam velocity $V = 0.5$ m/min. The structure with the planar front was 17 μm thick. The transition from this type of structure to a cellular one was observed at a dimensionless depth of 0.97. The initial dimensionless depth of the melted layer is equal to unity.

For $V = 1.0$ m/min , the morphological instability of the solidification interface is highly pronounced. Transitions depths are shown in Figure 4c (transition from a planar interface to a cellular structure and from a cellular to cellular-dendritic structure).

It was determined that the depth of the transition from cellular to cellular dendritic structure is dependent on the laser beam velocity (Table 2): the transition depth is decreasing with the beam velocity.

The following technique was applied for determining the $(G/R)_{cr}$ values. Using the measured values of transition depth, we plot the corresponding dimensionless depths values on the z/H axis of the G/R versus z/H plot (Figure 4a). The $(G/R)_{cr}$ value is further determined from the plot.

Thus, for the titanium alloy (wt%) Al 4.5, Mo 2.0, V 4.5, Cr 1.0, Fe 0.6 it was established that the region of the solidification planar front lies above $(G/R)_{cr1} = 1.5 \cdot 10^5\ K \cdot s/cm^2$; the $5.3 \cdot 10^4 - 1.5 \cdot 10^5$ K·s/cm^2 range corresponds to the zone of cellular structures and the range $(G/R)_{cr2} = 3.0 \cdot 10^4 - 5.3 \cdot 10^4$ K·s/cm^2 is related to the transition from a cellular to cellular dendritic structure.

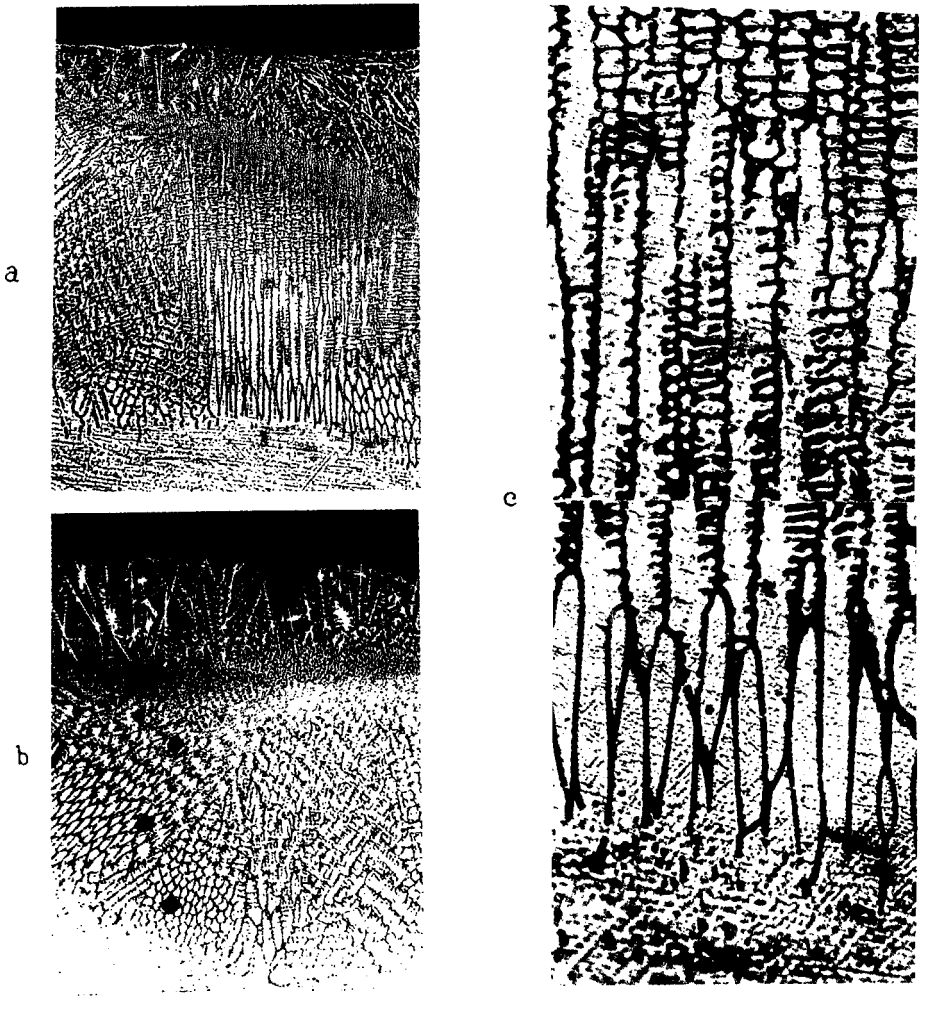

Fig. 5. Microstructure of titanium alloy after laser boriding with 1kW power, a - V = 1.0 m/min (× 200), b - V = 0.5 m/min (× 150), c - V = 1.0 m/min (× 1000) [4].

Table 2. The dependence of relative depth of transition from cellular to cellular-dendritic structure on laser beam velocity.

Laser beam velocity V, m/min	0.5	1.0	2.0
Relative depth of transition	0.6-0.8	0.8-0.9	0.9

5. Conclusions

The following regularities for the rapid solidification process in metallic alloys, in particular in Armco-iron and titanium alloy (wt %) Al 4.5, Mo 2.0, V 4.5, Cr 1.0, Fe 0.6, subjected to pulsed and CW-laser treatments have been established:

1. Common behavior of the G/R value at the solidification interface is approximately the same for continuous (Figure 4b) and pulse (Figure 3d) laser treatment. For CW-laser irradiation, G/R is at maximum at the onset of solidification, at z/H in the range from 1.0 to 0.9, it drastically drops and, further, at z/H in the range from 0.9 to 0 it smoothly decreases up to a certain V-dependent value. In the case of pulsed laser treatment, $G/R \to 0$ at the end of solidification process.
2. In the case of continuous laser treatment the G/R vs z/H curve, corresponding to a higher laser beam velocity, lies below the G/R curve with lower V.
3. The regularity established in [1] for Ni alloys has been verified: a successive transition from a planar front to a cellular structure and, further, from a cellular to cellular-dendritic structure is due to decrease of the G/R value during solidification.
4. It has been found that for the considered Ti alloy the region of planar solidification interface lies above $(G/R)_{cr1} = 1.5 \cdot 10^5\,\mathrm{K \cdot s/cm^2}$, the range $5.3 \cdot 10^4 - 1.5 \cdot 10^5\,\mathrm{K \cdot s/cm^2}$ corresponds to the region of cellular structures, the range $(G/R)_{cr2} = 3.0 \cdot 10^4 - 5.3 \cdot 10^4\,\mathrm{K \cdot s/cm^2}$ is related to the transition from a cellular to cellular-dendritic structure.
5. In the case of continuous laser treatment the depth of the transition from cellular to cellular-dendritic structure decreases with the laser beam velocity.
6. The character of the cooling rate $\dot{T}$ dependence on z/H at the solidification interface is approximately the same for pulsed and continuous laser treatment.

6. Acknowledgement

The research described in this publication was made possible in part by Grant from the Fundamental Research Funds of the Republic of Belarus.

7. Literature

1. GREENWALD L.E., BREINEN E.M., KEAR B.H., Laser-Solid Interaction and Laser Processing - 1978 (FERRIS S.D., LEAMY H.J., POATE J.M. eds.), Boston, USA (1979) 189-204.
2. ASTAPCHIK S.A., BERJEZA N.A., Izvestija AN BSSR, Ser. fiz.-tehnich. nauk, (1989) N 4, 23-29.
3. Physical Metallurgy R.W. CAHN (editor), Amsterdam, (1965).
4. BUSHIK S.V., BERJEZA N.A., VELIKEVICH S.P., Proceedings of the Intern. Conf. on Surface Modification Technologies-IV (SUDARSHAN T.S., BHAT D.G. and JEANDIN M.eds.), Paris, (1990) 771-782.
5. TSAREV G.L., LASKOVNEV A.P., BABUSHKIN V.B. Izvestija AN BSSR, Ser. fiz.-tehnich. nauk, (1986) N 3, 20-24.
6. KAR A. and MAZUMDER J., Acta Metall. 36 (1988) N.3, 701-712.
7. AZIZ M.J., J.Appl.Phys. 52 (1982) N.2,1158-1168.
8. CHALMERS B. Principles of Solidification. New Jork-London- Sydney (1966).
9. IVANTSOV G.P. Doklady AN SSSR, 81 (1951) N 2,179-182.
10. MULLINS W.W., SEKERKA R.F .J. Appl. Phys. 35 (1964) N 2, 444-451.
11. CORIELL S.R., SEKERKA R.F. J.Cryst.Growth, 19 (1973) N 4, 285-293.
12. CORIELL S.R., SEKERKA R.F. J. Cryst. Growth, 61 (1983) N 3, 499-508.
13. CAROLI B., CAROLI C., MISHBAH C., ROULET B.J. Physique, 46 (1985) N 3, 401-413.
14. JOUNG G.W., DAWIS S.H., BRATTKUS K.J. Cryst. Growth, 83 (1987) N 4, 560-571.
15. BRATTKUS K.,DAVIS S.H.J. Cryst. Grouth, 89 (1988) ,N.4, 423-427.
16. TRIVEDI R., KURZ W. Acta Metall. 34 (1986) N 8, 1663-1670.
17. Physical Metallurgy. CAHN R.W. and HAASEN P.(eds.) Amsterdam-Oxford-New Jork-Tokyo (1983) Vol.2.
18. ASTAPCHIK S.A., TSAREV G.L., BERJEZA N.A. and CHEBOTKO I.S. Izvestija AN BSSR, Ser. fiz.-tehnich. nauk, (1989) N.4, 23-29.
19. ASTAPCHIK S.A., BERJEZA N.A., Izvestija AN BSSR, Ser.fiz.-tehnich. naur, (1989) N.1, 29-32.

20. STRUTT P.R., LEWIS B.G., KEAR B.H., Critical Factors in Laser and Electron Beam Glazing of Materials (KEAR B.H., GIESSENB.C., COHEN M.eds.), Amsterdam. (1982) 485-495.
21. TILLER W.A., JACKSON K.A., RUTTER J.W., CHALMERS B. Acta Metall.1 (1953) 428-437.
22. TILLER W.A., RUTTER J.W., Canad. J. Phys. 34 (1956) N.1, 96-121.
23. RYKALIN N.N., UGLOV A.A., ZUEV I.V.KOKORA A.M. Laser and Electron-Beam Treatment of Material. Moscow (1985) 495.
24. ASTAPCHIK S.A.,VELIKEVICH S.P., Izvestija AN BSSR, Ser. fiz.-tehnich. nauk, (1988) N 4, 18-21
25. RYKALIN N.N. Computations of thermal processes in welding. Moscow (1951).
26. CLINE H.E. and ANTHONY T.R. J. Appl. Phys. 48 (1977) 3895-3900.

8. Nomenclature

T, T_s, T_0 – temperature, temperature of solidification, initial temperature
λ, a – thermal conductivity and thermal diffusivity
τ – laser pulse duration
$q(z,t)$ – internal heat source
q_{abs} – density of absorbed power
H, D – initial depth and width of melt
f, f_s – dimensionless temperature and temperature of solidification
f_0 – dimensionless temperature on the $y = 0$ plane
R_{ef}, P_{ef} – efficient radius and absorbed power of Gaussian source
q_{ef} – density of efficient absorbed power
$\vec{V}$ – velocity of laser beam, $V = |\vec{V}|$
ρ – dimensionless velocity of laser beam,
$\vec{G} = \nabla T$ – temperature gradient, $G = |\vec{G}|$
$\vec{R}$ – normal velocity of the interface, $R = |\vec{R}|$
α – corner between the $\vec{V}$ and $\vec{R}$
$\mathrm{erf}(x) = 1 - \mathrm{erfc}(x) = \dfrac{2}{(\pi)^{1/2}} \int_0^x \exp(-t^2)\, dt$ – error function
For any cartesian coordinate system (x_1, x_2, x_3) and
its ortonormal unit vector system $(\vec{e}_1, \vec{e}_2, \vec{e}_3)$
$\Delta = \sum_{i=1}^{3} \dfrac{\partial^2}{\partial x_i^2}$ – Laplas operator
$\nabla = \sum_{i=1}^{3} \nabla_{x_i} \cdot \vec{e}_i = \sum_{i=1}^{3} \dfrac{\partial}{\partial x_i} \cdot \vec{e}_i$ – nabla operator